Supporting Information

Bidirectional interfacial interactions and Cu_xS bond formation enabled by a thiourea-crosslinked binder for high-performance micro-SiO_x anodes

Jong Hyeok Han[a,b], Seo Jin Yeon[a,b], Chaeyoung Kim[a,b], Senthil Kannan[b], Taeeun Yim[b,c,],*

and Tae-Hyun Kim[a,b,]*

[a]Organic Material Synthesis Laboratory, Department of Chemistry, Incheon National University, Incheon, 22012, Republic of Korea.

[b]Research Institute of Basic Sciences, Incheon National University, Incheon, 22012, Republic of Korea.

[c]Advanced Batteries Laboratory, Department of Chemistry, Incheon National University, Incheon, 22012, Republic of Korea.

[*]Corresponding author. Tel: +82-32-835-8232; Fax: +82-32-835-0762; E-mail: yte0102@inu.ac.kr (T. Yim), tkim@inu.ac.kr (T.-H. Kim)

Materials

Acrylamide (AM), acrylic acid (AA), and potassium persulfate (KPS) were purchased from Sigma-Aldrich (St. Louis, MO, USA), CMC (carboxyl methyl cellulose), SiO_x (1400 mAh g^{-1}, **Fig. S1**), Super C, Cu current collector, separator (polyethylene, PE), lithium metal, and the electrolyte were provided by Hyundai Motor Company.

Preparation of binder solution

Initially, high-purity nitrogen gas was bubbled into the solvent to remove dissolved oxygen. Subsequently, acrylamide and acrylic acid, both purified to remove inhibitors, were dissolved in the nitrogen-purged solvent according to a specified weight ratio. Potassium persulfate (KPS, 0.5 wt%) was added as a radical initiator. The sealed flask was stirred at 60 °C for 12 h to initiate polymerization, resulting in a viscous solution. After the reaction, the product was precipitated using acetone and washed several times to remove impurities. The purified copolymer, poly(acrylic acid-co-acrylamide) (PAAAM), was then dried under vacuum at room temperature for 12 h. For crosslinking, the synthesized PAAAM and thiourea were mixed at a weight ratio of 95:5, and the mixture was stirred in deionized water (5 wt%) at room temperature for 24 h to prepare the x-PAAAM-Tu binder solution.

Preparation of SiO_x electrode

SiO_x, binder, and Super C were mixed and dispersed in a weight ratio of 8:1:1. The resulting electrode slurry was coated onto copper foil using the doctor blade method, achieving a mass loading of 1.3–5.3 mg cm^{-2}. The coated electrodes were initially dried at 120 °C for 10 mins, followed by calendaring to obtain an electrode composite density of 1.1–1.2 mg cm^{-3}. Circular electrodes (12 mm in diameter) were then punched and further dried under vacuum at 120 °C for 12 h to remove residual moisture. The half-cells were assembled in an argon-filled glove box using

lithium metal as the counter electrode. A formation process consisting of three charge-discharge cycles was conducted at 0.1 C for 12 h per cycle. Subsequently, electrochemical performance was evaluated under various charge-discharge rates in the range 1.0−5.0 C. The full cell was prepared with $LiNi_{0.8}Co_{0.1}Al_{0.1}O_2$ (NCA 811) as the cathode and the SiO_x-based electrode as the anode. The cathode was fabricated by mixing NCA 811, the polyvinylidene fluoride (PVDF) binder, and Super C in a ratio of 96:2:2 (wt%) using *N*-methyl pyrrolidone (NMP) as the slurry solvent. The electrodes were oven-dried for 3 h at 120 °C. The 10 ϕ-sized electrodes were then dried at 120 °C for 12 h under vacuum to remove any residual solvent. The NCA cathode mass loading was set to 16–20 mg cm^{-2}, and the N/P ratio between the anode and cathode was 1.05–1.1. The full cell was charged/discharged in the voltage range of 3.0–4.3 V at 0.1 C for three cycles, after which the charge/discharge currents were increased to 1.0/1.0 C for 200 cycles.

Characterization and measurement

^1H NMR spectra were obtained using an Agilent 400-MR (400 MHz) instrument using D_2O as a solvent. Fourier transform infrared (FTIR) spectra were acquired with a Spectrum Two ATR spectrometer (PerkinElmer, Waltham, MA, USA) to examine changes in the functional groups.

The polymer's inherent viscosity (η) was measured at 25 ℃ using an AVS 370 viscometry measuring system (Schott, Germany) using 0.01 wt% polymer solution. η_{inh} was calculated using Equation S1:

$$\eta_{inh} = \frac{\left(\frac{t_1}{t_0} - 1\right)}{c} \#(Eqaution\ S1)$$

where t_1 is the outflow time of the polymer solution, t_0 is the outflow time of the solvent, and c is the polymer concentration.

A Surface and Interfacial Characterization Analysis System (SAICAS EN-EX, Daipla Wintes, Japan) was used to measure the adhesion and cohesion strength. Peel testing and nanoindentation were used to determine the mechanical properties of the Si electrodes. The electrodes were prepared with 12 mm-wide 3M tape for the peel test. The adherence of SiO_x and Super C to the polymeric binder was measured using a universal testing machine (UTM, Shimadzu, Japan) at a constant displacement rate of 30 mm min^{-1}. The nanoindentation was measured using a Nano indenter (KLA-Tencor, USA) with SiO_x electrode composite layers. The maximum indentation load was 0.8 mN, and the nanoindentation was completed at a constant strain rate of 0.05 nm s^{-1}. A rheometer (ARES-G2, TA Instruments, USA) was used to measure the viscoelastic behavior. Contact angle measurements were carried out in static mode using a surface electro-optics (SEO) instrument and analyzed with SEO Surfaceware-9 software. For each measurement, the electrode was mounted on carbon tape, a 5-µL droplet of electrolyte was dispensed onto the electrode surface, and an image was captured directly after contact to determine the contact angle.

Field emission scanning electron microscopy (FE-SEM; JEOL JSM-7800F, Japan) was performed to investigate the morphology of the electrodes before and after cycling. Cross-sectional analysis of the electrode thickness was conducted by disassembling the cell after 100 cycles under similar conditions, removing the residual electrolyte using dimethyl carbonate (DMC) as a washing solvent, and obtaining cross-sectional images from the central region of the electrodes. To ensure reproducibility, the measurements were performed in triplicate, and the image showing the maximum thickness was selected. X-ray photoelectron spectroscopy (XPS) was conducted using a PHI 5000 Versa probe-II (ULVAC-PHI, Inc., Japan) with a monochromatic Al-Kα X-ray source at a take-off angle of 90° to the surface plane. High-resolution scans of C_{1s}, N_{1s}, O_{1s}, F_{1s}, S_{2p}, Cu_{2p}, and Si_{2p} were recorded using a pass energy of 5 eV, and the XPS peaks were detected using XPS 41. The surface morphology and height variation of the uncompressed SiO_x electrodes were characterized using 3D-surface confocal laser scanning microscope(3D-LSM, OLS5100).

Electrochemical testing

A 2032-type coin cell was used to test the electrochemical performance in an Ar-filled glove box (O_2 < 0.01 ppm, H_2O < 0.01 ppm). Porous polyethylene was used as the separator, and lithium metal disks as the counter and reference electrodes. Using a CPS-Lab battery cycler (BaSyTec, Germany) at 27 °C in a temperature-controlled chamber, all the cells were charged to 0.02 V (vs. Li/Li^+) using the constant current/constant voltage (CC/CV) technique and discharged to 1.6 V (vs. Li/Li^+) using the constant current (CC) method.

Electrochemical impedance spectroscopy (EIS) and cyclic voltammetry (CV) were performed using an electrochemical potentiostat/galvanostat system (VSP, BioLogic, France). The EIS spectra were obtained at an AC amplitude of 10 mV over a frequency range of 100 kHz to 10 MHz, and CV was conducted with a scanning voltage of 0.1 mV s^{-1}. Lithium diffusion coefficients using scan rate were calculated using the Randles-Sevcik equation (Equation S2):

$$i_p = (2.69 \times 10^5) n^{3/2} A C D^{1/2} v^{1/2} \#(Eqaution\ S2)$$

where v is the scan rate, i_p is maximum current density, A is the area of the electrode, n is number of electrons transferred, and C is the concentration of Li^+.

Lithium diffusion coefficients were calculated using the Warburg equation (Equation S3):

$$D_{Li} = \frac{R^2 T^2}{2A^2 \times n^4 F^4 C^2 \sigma^2} \#(Eqaution\ S3)$$

where σ is the Warburg coefficient, R is the gas constant, T is the temperature, n is number of electrons transferred, A is the area of electrode, F is the Faraday constant, and C is the concentration of Li^+.

GITT tests were conducted in the voltage range of 0.01–1.6 V, using a 10-minute current pulse followed by a 30-minute rest period. The lithium diffusion coefficients were then calculated from the scan rate using Equation S4.

$$D_{Li} = \frac{4}{\pi\tau}\left(\frac{n_m V_m}{S}\right)^2\left(\frac{\Delta E_s}{\Delta E_t}\right)^2 \#(Eqaution\ S4)$$

where τ is the galvanic titration time, n_m is the number of mole, V_m is the molar volume, S is the electrode area, ΔE_s is total voltage change due to the pulse, ΔE_t is Voltage change during constant current charging/discharging.

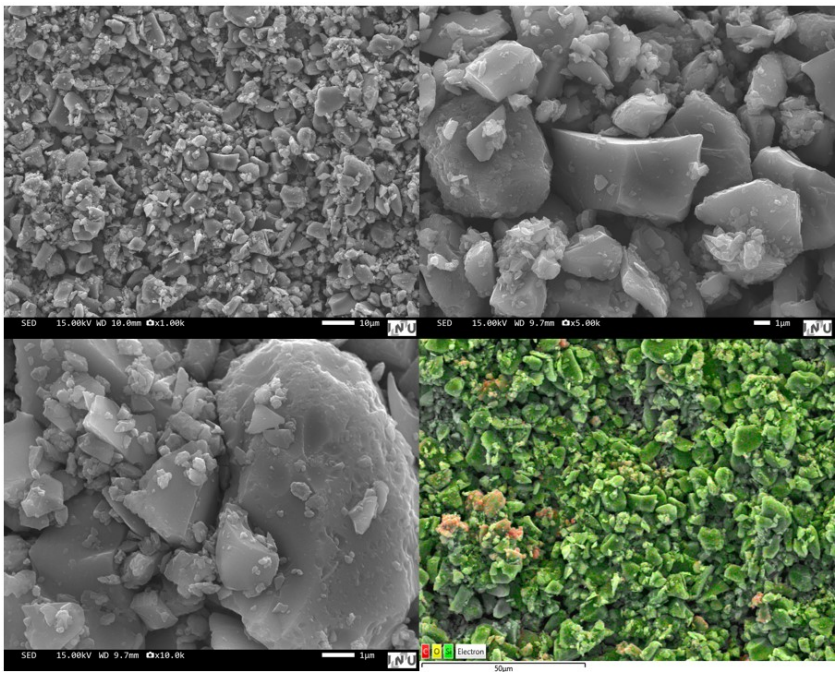

Fig. S1. Scanning electron microscopy (SEM) images of SiO_x powders.

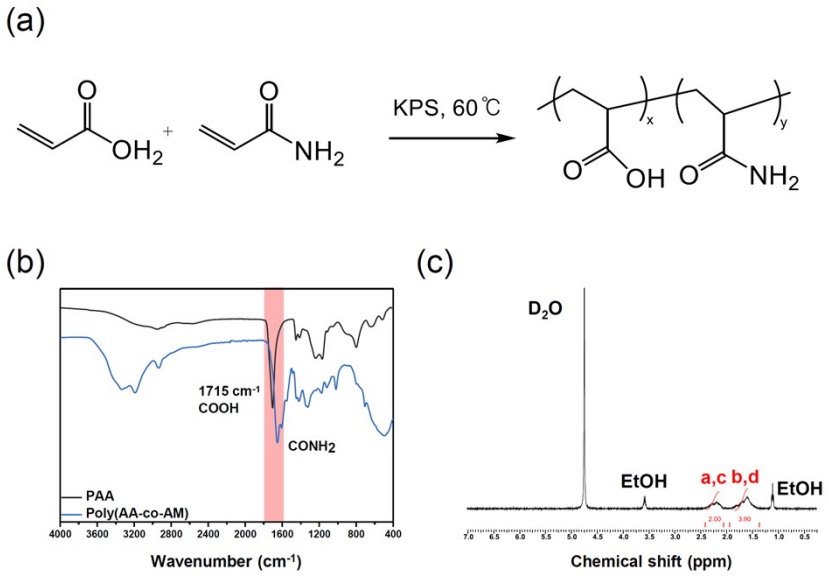

Fig. S2. Characterization of AA-co-AM: (a) Schematic illustration of synthesis of Poly(AA-co-AM) copolymer. (b) Fourier transform infrared (FT-IR) spectra of PAA and Poly(AA-co-AM). (c) ^{1}H NMR spectra of the poly(AA-*co*-AM) carried out in D_2O solution.

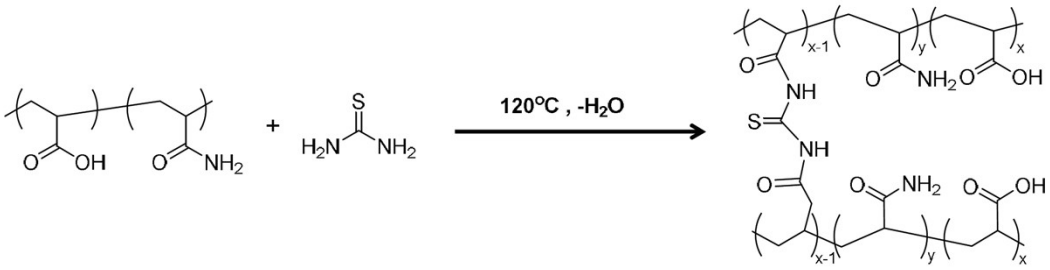

Fig. S3. Schematic illustration of synthesis of x-PAAAM-Tu.

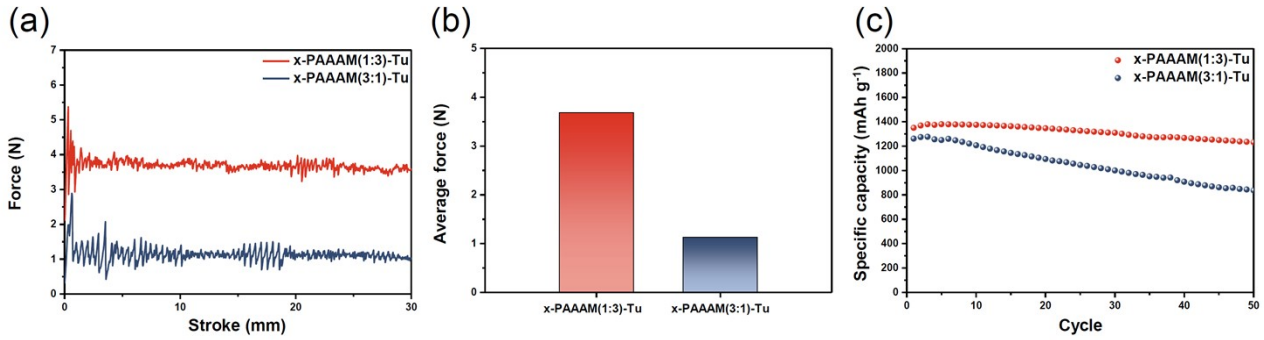

Fig. S4. Evaluation of electrode properties of x-PAAAM-Tu with different co-monomer compositions: (a,b) peel-off tests of x-PAAAM(1:3)-Tu and x-PAAAM(3:1)-Tu; and (c) electrochemical performance at 1.0 C for x-PAAAM(1:3)-Tu and x-PAAAM(3:1)-Tu.

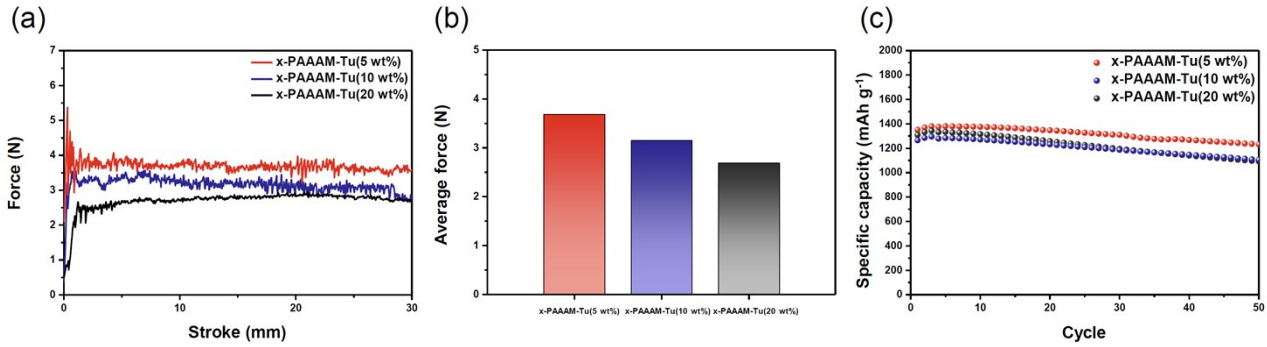

Fig. S5. Evaluation of electrode characteristics with varying thiourea (Tu) crosslinker contents: (a,b) peel-off tests of x-PAAAM-Tu (5, 10, and 20 wt%); and (c) electrochemical performance at 1.0 C for x-PAAAM-Tu with 5, 10, and 20 wt% crosslinker content.

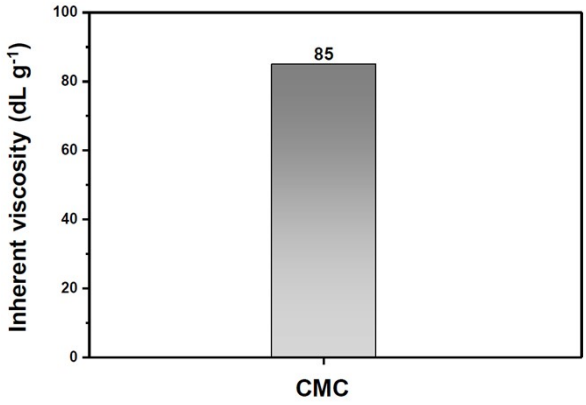

Fig S6. Inherent viscosity of CMC.

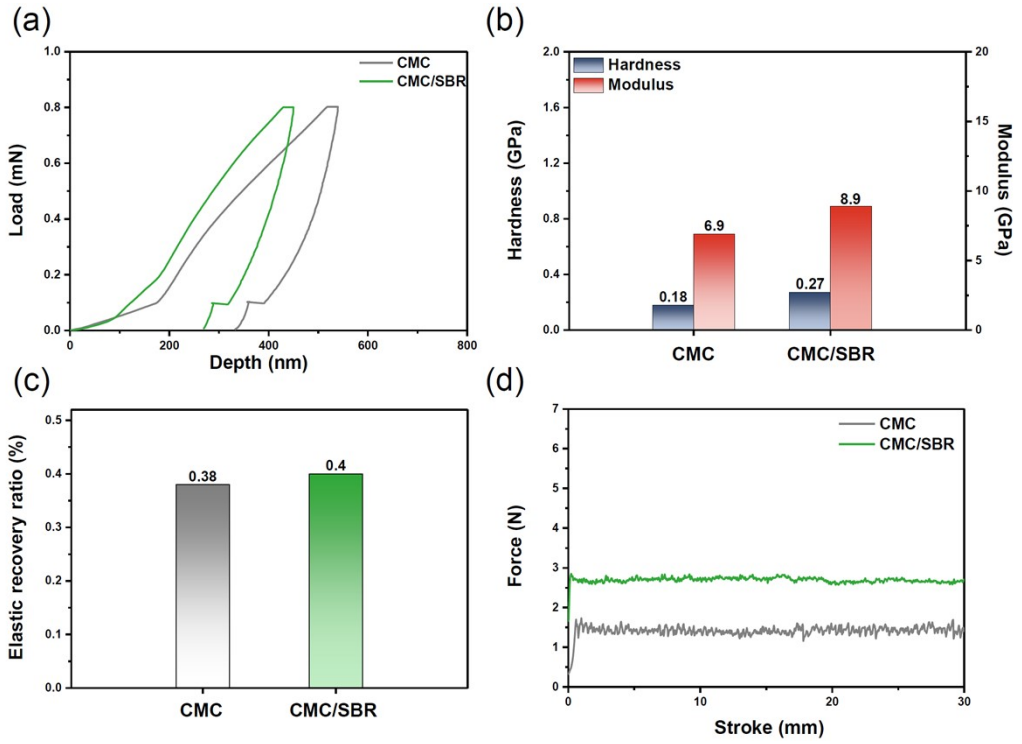

Fig. S7. Mechanical properties of CMC/SBR and CMC binders: (a) Nanoindentation profiles, (b) hardness and modulus data, (c) elastic recovery ratio, and (d) 180° peel-off test of CMC/SBR and CMC.

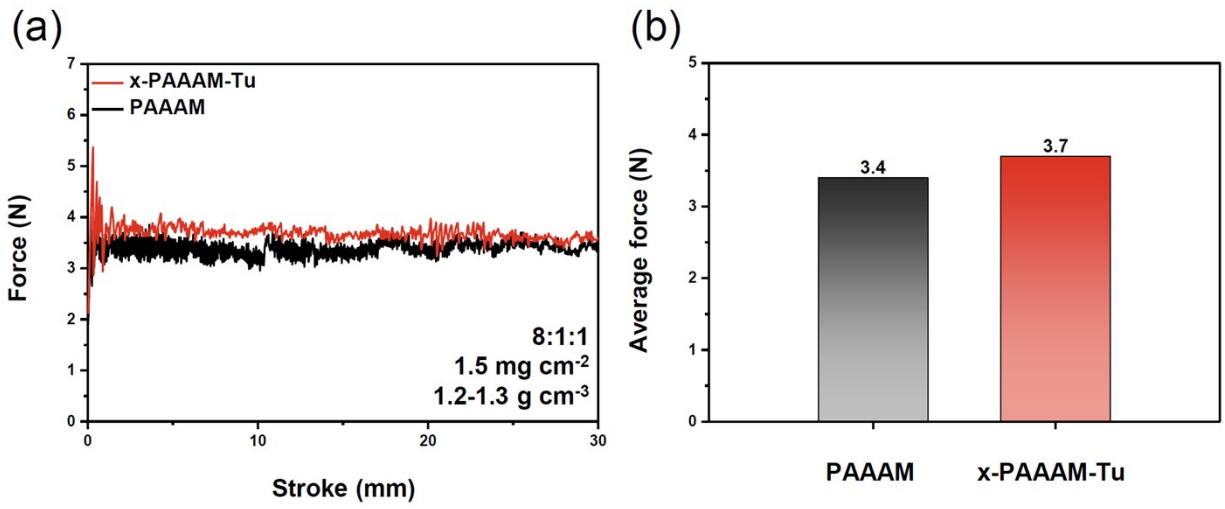

Fig. S8. Adhesion evaluation under general evaluation conditions: (a) peel-off test of low loading x-PAAAM-Tu and PAAAM; and (b) average peel strength.

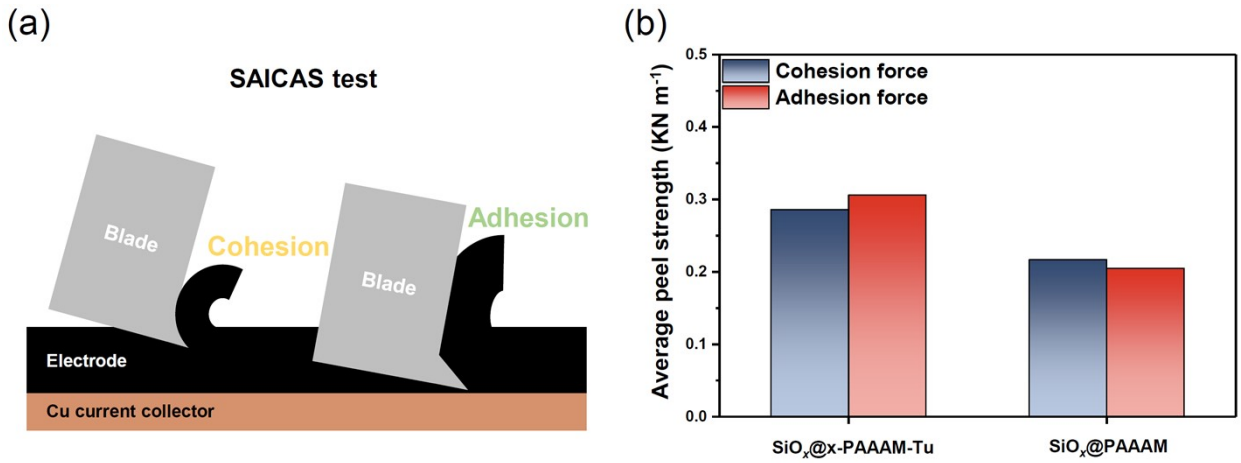

Fig. S9. Evaluation of SAICAS: (a) schematic illustration of SAICAS test; and (b) average peel strength of SiO_x@x-PAAAM-Tu and SiO_x@PAAAM.

Fig S10. Digital photographs of the x-PAAAM-Tu, PAAAM, and CMC electrodes before (top) and after (bottom) soaking for 7 days and sonication for 6 hours.

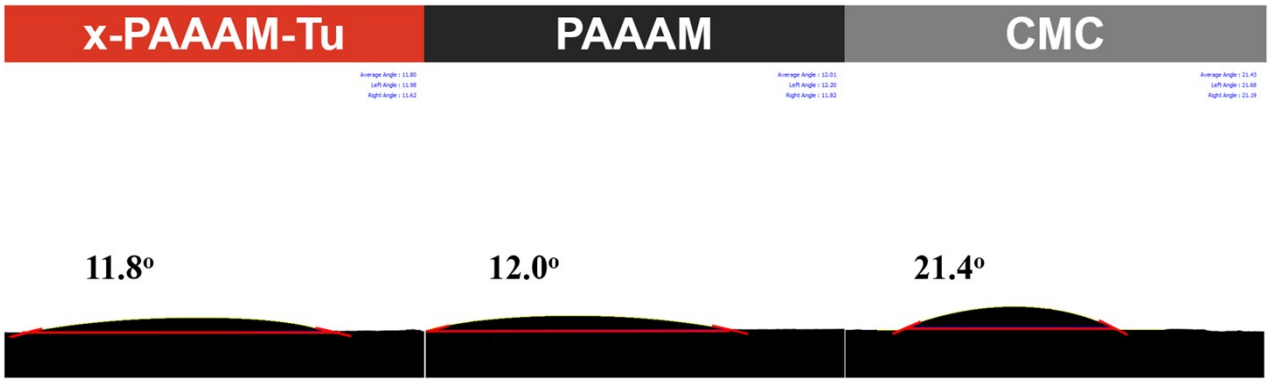

Fig S11. Contact angle data of the x-PAAAM-Tu, PAAAM, and CMC electrodes using the electrolyte.

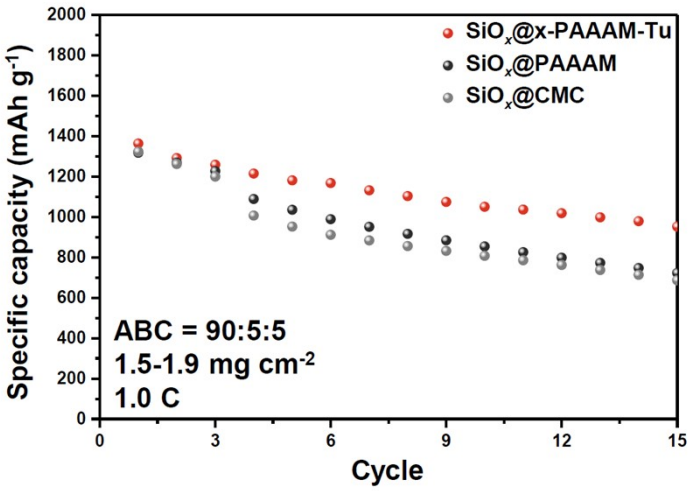

Fig. S12. Electrochemical performance of SiO_x@x-PAAAM-Tu, SiO_x@PAAAM, and SiO_x@CMC electrodes with a 90:5:5 (active material:binder:Super C) composition**.**

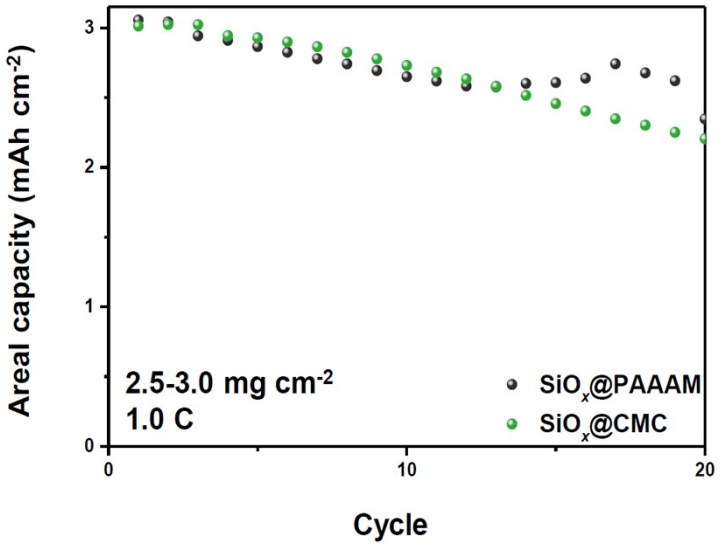

Fig S13. Cycling performance of SiO_x@PAAAM and SiO_x@CMC electrodes under high mass-loading conditions.

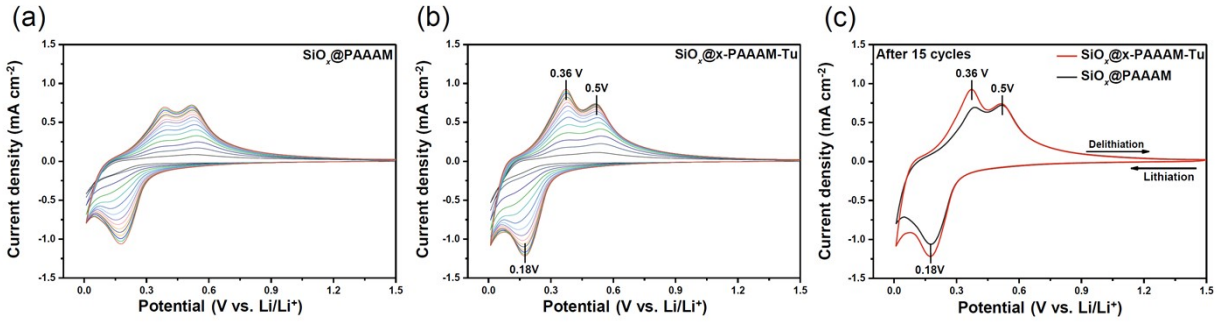

Fig. S14. Cyclic voltammetry curves of SiO_x electrodes using PAAAM and x-PAAAM-Tu binders.

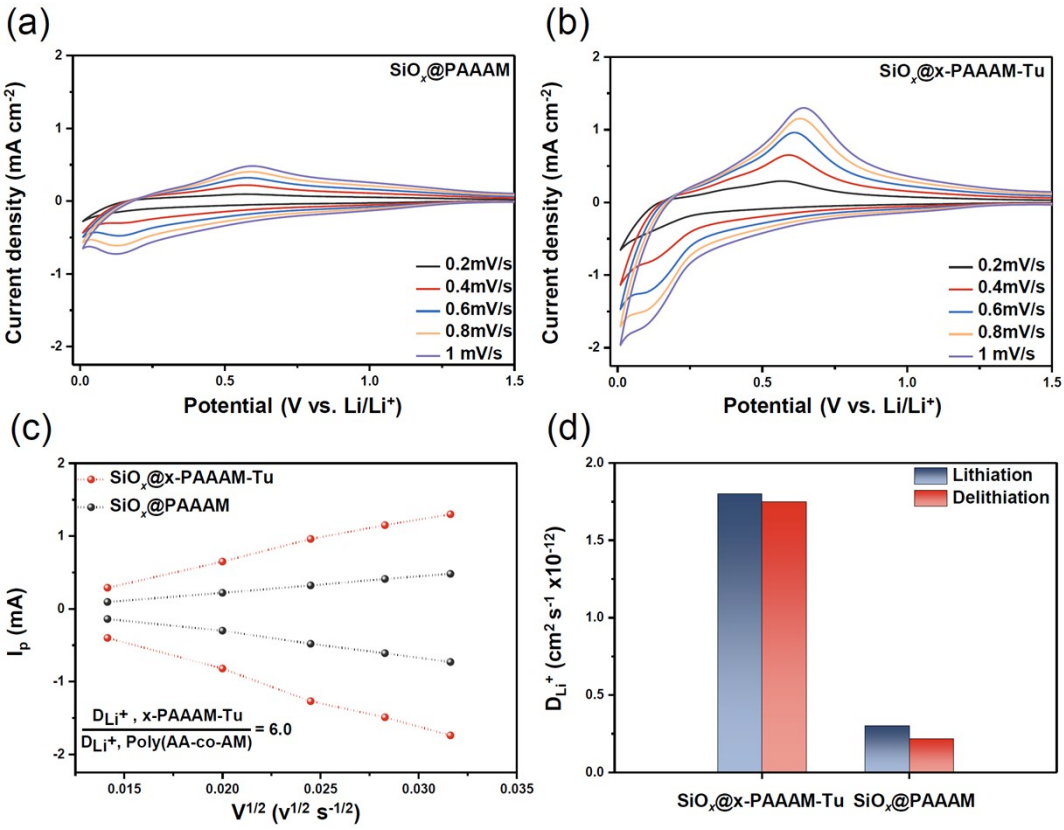

Fig. S15. Electrochemical properties of the SiO_x electrodes using x-PAAAM-Tu and PAAAM: (a,b) cyclic voltammetry curves at different scan rates from 0.2 mV s^{-1} to 1.0 mV s^{-1}; (c) the relationship of peak current (Ip) versus square root of potential scanning rates ($v^{0.5}$); and (d) lithium diffusion coefficient (D_{Li}^{+}) of x-PAAAM-Tu and PAAAM using CV.

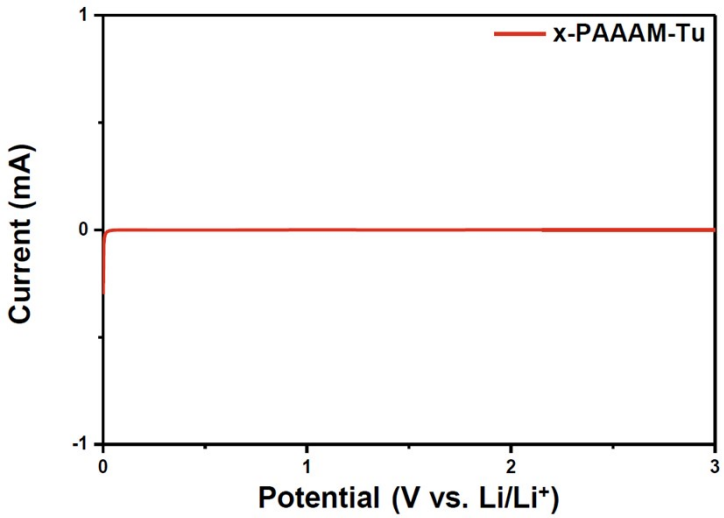

Fig. S16. Linear sweep voltammetry of x-PAAAM-Tu.

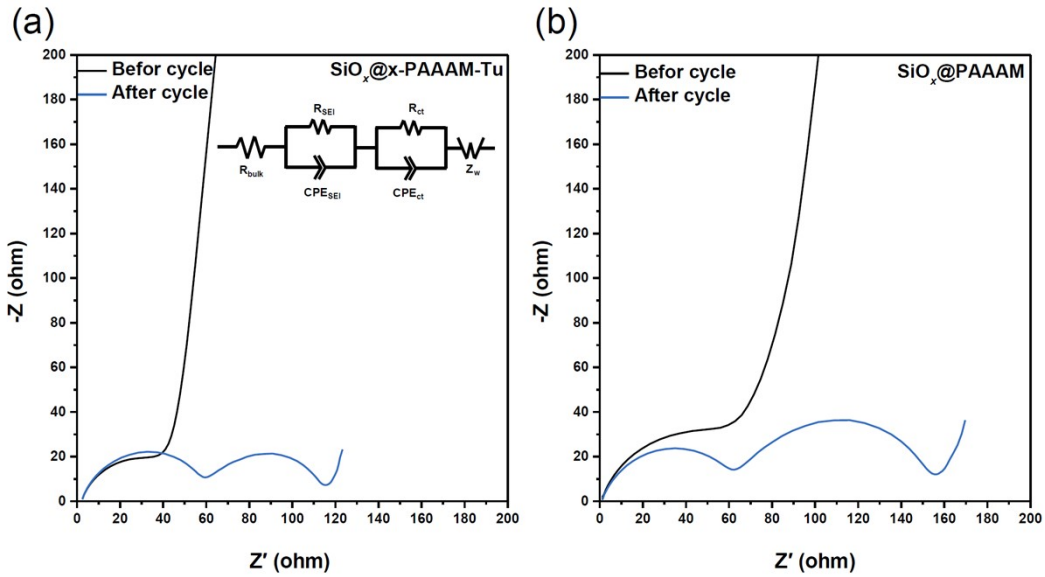

Fig. S17. Electrochemical impedance spectra before and after the formation cycle of (a) SiO_x@x-PAAAM-Tu and (b) SiO_x@PAAAM.

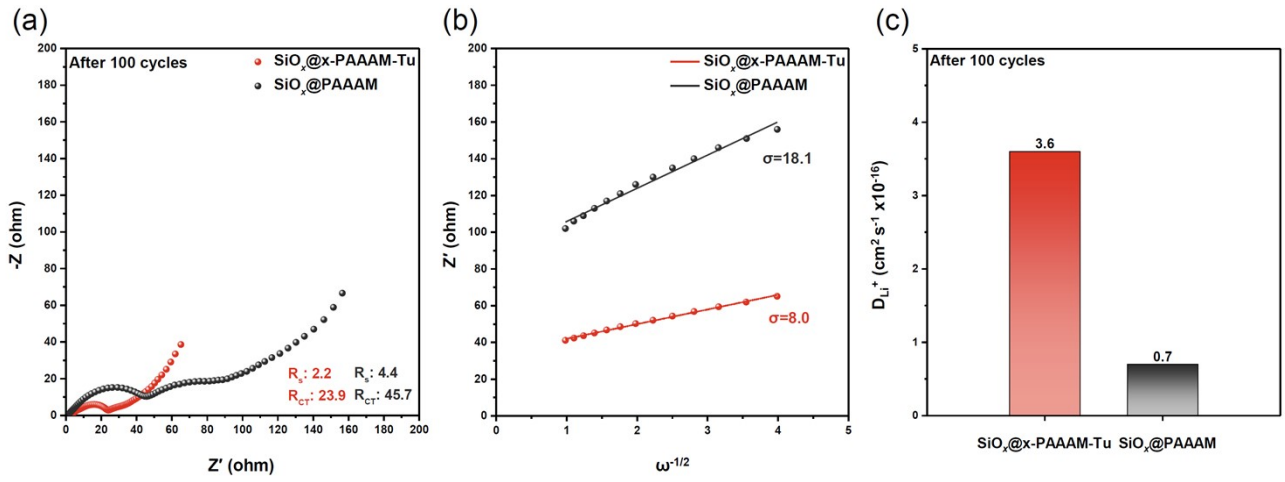

Fig. S18. Electrochemical impedance spectra of SiO_x@x-PAAAM-Tu and SiO_x@PAAAM: (a) after 100 cycled electrochemical impedance spectra; (b) Warburg impedance values from EIS; and (c) lithium diffusion coefficient (D_{Li}^+) of x-PAAAM-Tu and PAAAM using Warburg slope.

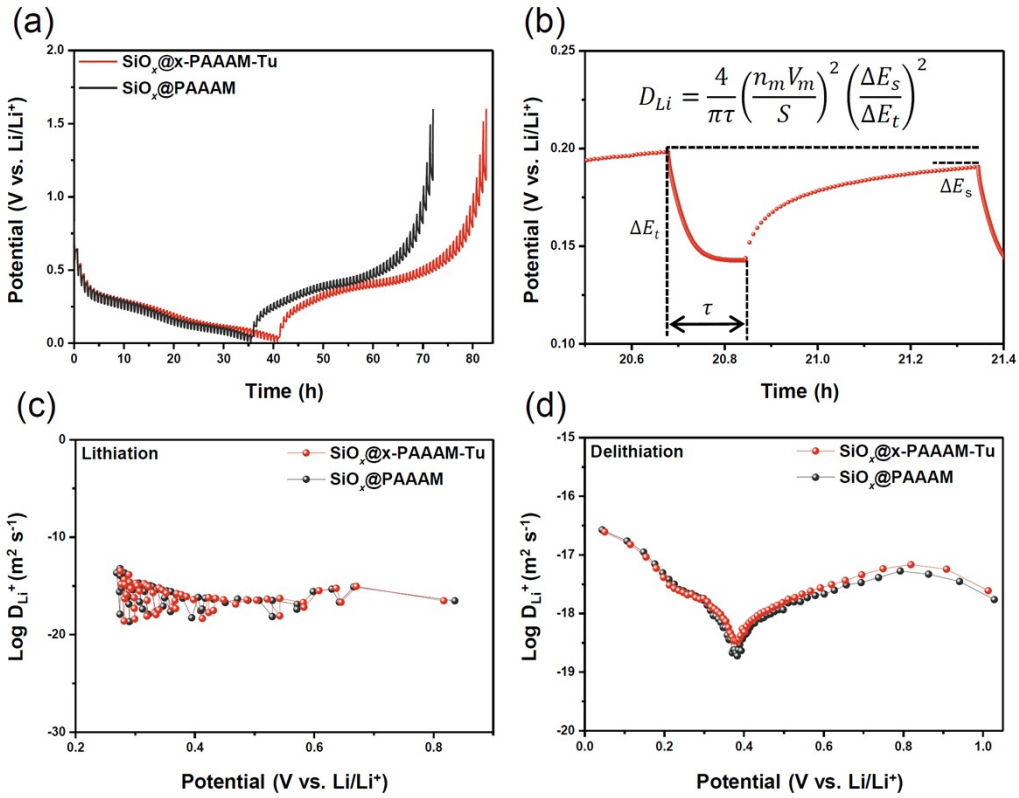

Fig. S19. Galvanostatic intermittent titration technique (GITT) results: (a) GITT curves of SiO_x electrode after 50 cycled, (b) schematic diagram for calculating lithium diffusion coefficient (D_{Li}^+); and D_{Li}^+ of x-PAAAM-Tu and PAAAM electrodes (c) lithiation, (d) delithiation.

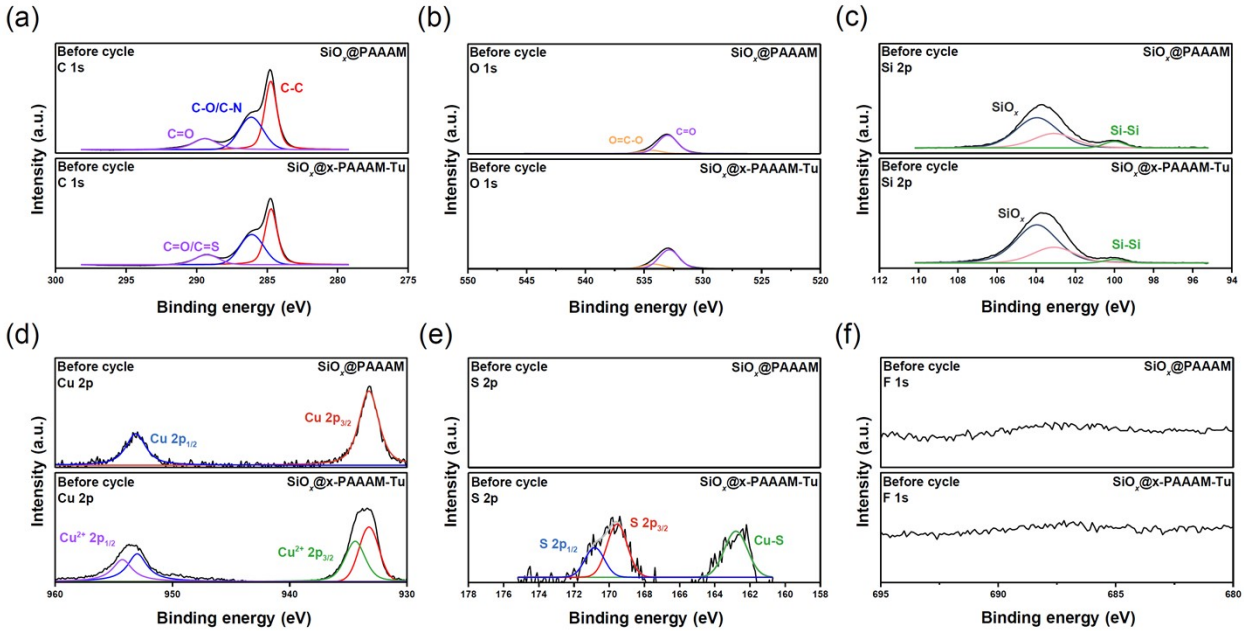

Fig. S20. X-ray photoelectron spectroscopy (XPS) spectra before cycling of SiO_x@PAAAM and SiO_x@x-PAAAM-Tu electrodes: (a) C_{1s}; (b) O_{1s}; (c) Si_{2p}; (d) Cu_{2p}; (e) S_{2p}; and (f) F_{1s}.

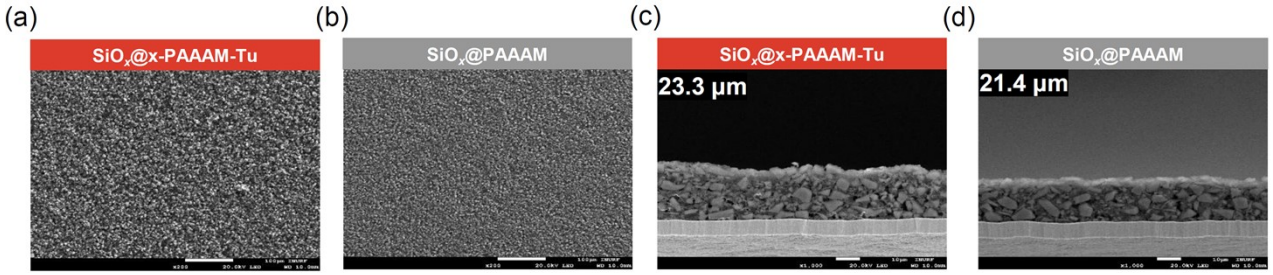

Fig. S21. SEM (scanning electron microscope) images before cycling of the electrodes: (a,b) surface images of SiO_x@x-PAAAM and SiO_x@PAAAM; and (c,d) cross-section images of SiO_x@x-PAAAM and SiO_x@PAAAM.

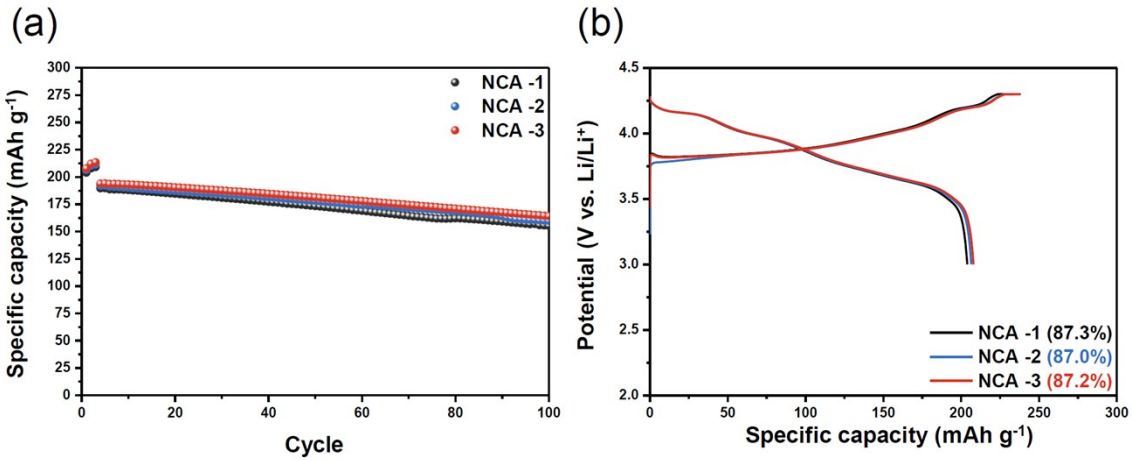

Fig. S22. Electrochemical performance of NCA 811 half cell: (a) cycling performance at current density 1.0 C; and (b) initial potential profile.

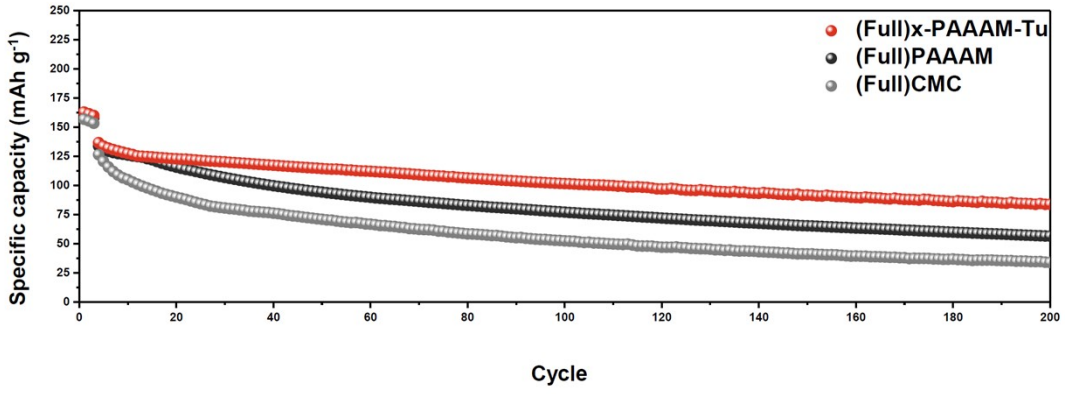

Fig. S23. Long cycle performance of NCA 811//SiO_x@x-PAAAM-Tu, NCA 811//SiO_x@PAAAM, and NCA 811//SiO_x@CMC electrodes.

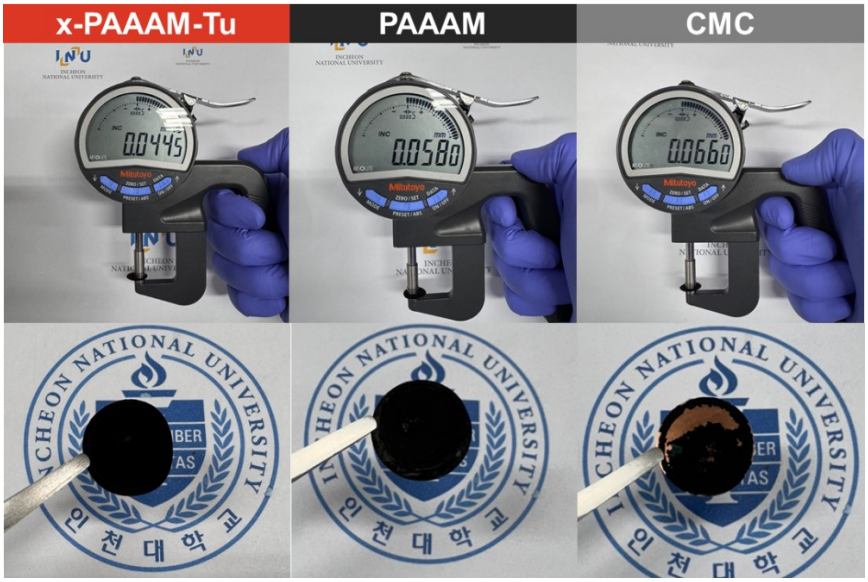

Fig. S24. Digital photographs of electrode thickness and morphology after 200 cycles.

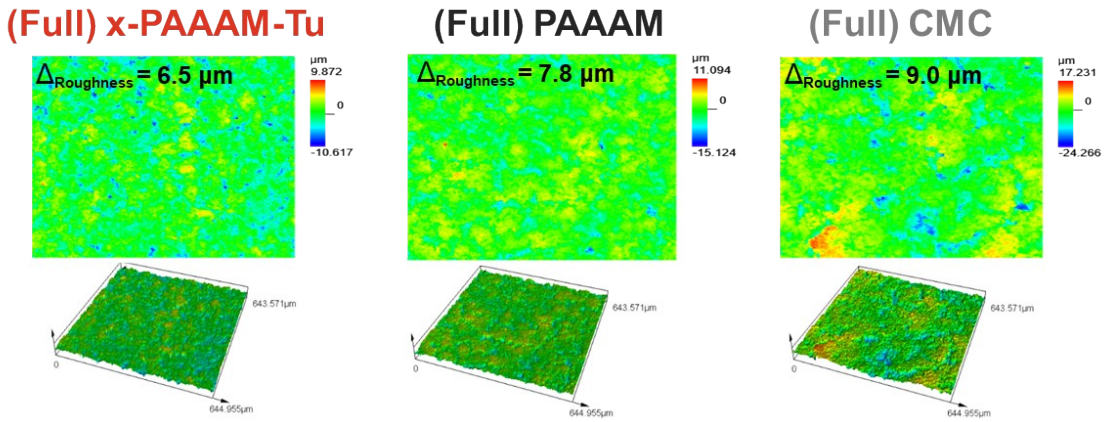

Fig. S25. 3D-laser confocal microscopy images after 200 cycles.

Table S1. Inherent viscosities (dL g^{-1}) for 0.01 wt% solutions of CMC, PAAAM, and x-PAAAM-Tu.

	Average flow time (s)	Relative viscosity	Inherent viscosity (dL g^{-1})
CMC	636.0	2.3	85.0
PAAAM	421.4	1.5	43.0
x-PAAAM-Tu	459.7	1.7	51.7

Table. S2. Comparison of cell performances of x-PAAAM-Tu and Si anodes with various polymer binders (reported in the literature) in terms of Si particle size and loading rate.

Binder	Type	Ratio (A:B:C)	Loading level (mg cm^{-2})	ICE (%)	Electrochemical performance	Ref.
SA5H5	SiO_x/Gr	80:10:10	1.6	81.3	506.2 mAh g^{-1} (66.7%) @ 0.5 C, 200 cycles	1
T-PGA	SiO	70:10:20	1.0	64.9	973.0 mAh g^{-1} (71.9%) @ 0.5 A g^{-1}, 500 cycles	2
Li0.75PAA	SiO_x	70:20:10	0.8–1.1	67.2	922.0 mAh g^{-1} (61.5%) @ 0.5 C, 400 cycles	3
PAA-LS	SiO_x	70:10:20	1.5–2.0	64.0	997.3 mAh g^{-1} (47.8%) @ 0.5 A g^{-1}, 450 cycles	4
CNTB	SiO_x	85:7.5:7.5	2.5–3.0	71.5	1709.9 mAh g^{-1} (91.0%) @ 0.5 C, 30 cycles	5
P(AA-co-LiAMPS)	SiO_x	60:20:20	1.3	68.0	587.8 mAh g^{-1} (52.0%) @ 1.0 C, 400 cycles	6
1PAA@1DOU	SiO_x	60:20:20	1.3	70.6	1322.9 mAh g^{-1} (83.7%) @ 0.5 C, 300 cycles	7
P2G1-150	Si/C	70:15:15	0.6–1.0	82.7	743.0 mAh g^{-1} (94.6%) @ 1.0 C, 200 cycles	8
PM 11	Si/C	70:10:20	-	75.0–80.0	483.5 mAh g^{-1} (53.8%) @ 0.5 C, 200 cycles	9
P31	SiO_x	60:20:20	1.3	72.7	882.9 mAh g^{-1} (47.3%) @ 0.1C, 150 cycles	10
GG-PAA	SiO_x	70:10:20	1.0	75.09	1153.8 mAh g^{-1} (75.4%) @ 0.5 A g^{-1}, 80 cycles	11
x-PAAAM-Tu	SiO_x	80:10:10	1.3–5.3	85.5	1134.7 mAh g^{-1} (87.2%) @ 1.0 C, 100 cycles 931.5 mAh g^{-1} (71.5%) @ 1.0 C, 300 cycles	**This work**

	Electrode loading level (mg cm^{-2})	Pristine electrode thickness (μm)	Electrode thickness after 200 cycles (μm)	Electrode thickness change ratio (%)
x-PAAAM-Tu	3.0	33.8	44.5	31.7
PAAAM	2.9	34.1	58.0	70.1
CMC	2.9	33.9	66.0	94.7

Table S3. Electrode thickness information before and after 200 cycles.

Reference

1. B. Dong, H. Zhu, X. Cai, C. Guo, Y. Hao, L. Xi, Rational design of alginate-derived network binder for high-performance silicon-based anodes in Li-ion batteries, J. Power Sources 626 (2025).
2. C. Huang, J. Liang, H. Xiao, et al., Cross-linking γ-Polyglutamic Acid as a Multifunctional Binder for High-Performance SiOx Anode in Lithium-Ion Batteries, ACS Appl. Mater. Interfaces 16 (2024) 62121–62130.
3. Z. Li, W. Tang, Y. Yang, et al., Engineering Prelithiation of Polyacrylic Acid Binder: A Universal Strategy to Boost Initial Coulombic Efficiency for High-Areal-Capacity Si-Based Anodes, Adv. Funct. Mater. 32 (2022).
4. M. Xu, X. Wei, Z. Yan, et al., A Fast Self-Healing Binder for Highly Stable SiOx Anodes in Lithium-Ion Batteries, ACS Appl. Mater. Interfaces (2024).
5. C. Ha, J.K. Koo, J.M. Sheem, Y.J. Kim, Enhancing micro-scale SiOx anode durability: Electro-mechanical strengthening of binder networks via anchoring carbon nanotubes with carboxymethyl cellulose, J. Energy Chem. 101 (2025) 23–33.
6. Z. Weng, G. Wu, J. Li, et al., Sulfonic Group Modified Binder Endows Rapid Lithium-Ion Diffusion for SiOx Microparticle Anode, Small Sci. 4 (2024).
7. G. Wu, Z. Weng, J. Li, et al., Body Armor-Inspired Double-Wrapped Binder with High Energy Dispersion for a Stable SiOx Anode, ACS Appl. Mater. Interfaces 15 (2023) 34852–34861.
8. L. Liu, H. Guo, Y. Yu, Q. Zhang, Y. Liu, N. Li, An esterified cross-linked polymer binder for high-rate stabilised silicon anodes in lithium-ion batteries, Electrochim. Acta 519 (2025).

9. H.J. Son, B.S. Reddy, H.J. Na, et al., An elastic cross-linked polymeric binder for high-performance silicon/graphite composite anodes in lithium-ion batteries, J. Alloys Compd. 1010 (2025).
10. Z. Weng, S. Di, L. Chen, et al., Random Copolymer Hydrogel as Elastic Binder for the SiO xMicroparticle Anode in Lithium-Ion Batteries, ACS Appl. Mater. Interfaces 14 (2022) 42494–42503.
11. R. Li, Z. Yang, Y. Liu, et al., Engineering self-adaptive composite binders for micron-sized SiOx in lithium-ion battery anodes, J. Power Sources 642 (2025).